Controlling light emission of nanoparticles

Lesage, A.

Publication date
2019
Document Version
Other version
License
Other

5

Hot-carrier-mediated impact excitation of Er^{3+} ions in SiO_2 sensitized by Si nanocrystals

Past research has shown that indirect excitation of Er^{3+} *ions in* SiO_2 *solid-state matrix with Si nanocrystals can be achieved by different pathways. Here, we investigate the impact excitation mechanisms in detail by means of time-resolved photoluminescence spectroscopy. We explicitly demonstrate that the free carrier impact excitation mechanism is activated as soon as the carriers obtain sufficient excess energy. The "hot" carriers with the above-threshold energy can be created upon optical pumping in two ways: either upon absorption of (i) a single photon with an energy exceeding a certain threshold* $h\nu > E_{\mathrm{th}}$ *or (ii) following absorption of multiple photons of lower energy in a single nanocrystal,* $h\nu < E_{\mathrm{th}}$*, followed by an Auger recombination of the generated multiple e-h pairs. In addition, we show that the impact excitation dynamics by hot carriers are similar, regardless of the mode in which they have been created.*

5.1 Introduction

Featuring $1.5\,\mu m$ emission coincident with the absorption minimum of optical fibers, Er-doped materials are broadly explored for, and applied in, telecommunication networks. The emission arises from radiative transitions between J states of the incomplete 4f electron shell of trivalent erbium ions (Er^{3+}). [101] Due to the effective screening of the 4f shell by the complete outer 5s and 5p orbitals, the host has only a very limited influence on the energy structure of the Er^{3+} ions; consequently a narrow emission band with a temperature invariant wavelength can be observed up to room temperature. However, transitions between the individual J states are only weakly allowed, yielding very long radiative lifetimes ($\approx$ ms) and very small optical absorption cross-sections for resonant excitation [102]. Consequently, excitation of Er-doped insulating materials can only be achieved by resonant pumping with high-power tunable lasers, which is cumbersome and energy-inefficient. Past research revealed that the excitation cross-section of Er^{3+} ions in SiO_2 can be increased by up to three orders of magnitude by co-doping with Si nanocrystals (NCs). In contrast to Er, Si NCs feature a larger absorption cross section over a wide energy range. Moreover, when in direct neighborhood of each other, a strong coupling appears between the Si NC and the Er^{3+} ions, leading to an effective sensitization of Er^{3+} emission. [9, 103–105] In this case, the Si NC absorbs a photon and due to the relatively long excited state life time, it can transfer its energy non-radiatively to an Er^{3+} ion, promoting it to one of its excited states. The sensitization effect of the $1.5\,\mu m$ Er-related emission, [104, 106–108] opened perspectives for Er-doped SiO_2 with possible application for broad-band flash lamp pumped amplifiers and lasers for telecommunication networks, but also a wide range of other applications, such as laboratory-on-a-chip, optoelectronics, all Si lasers [109] and also future photovoltaics. [37, 110]

The sensitization process has been extensively investigated and modeled, [111–113] but a full understanding hereof, and thus optimization, remains challenging. It has been shown that only Er^{3+} ions in the vicinity of a Si NC can be indirectly excited via Si NCs, and those constitute a minor fraction of the total Er concentration embedded in the material. By dedicated experiments, it was revealed that in optimized materials only approximately 1% of the overall concentration of Er^{3+} could be indirectly excited via Si NCs. While later attempts increased that percentage somewhat, [114] it remained low, thus precluding realization of population inversion, and optical gain [115].

The energy transfer between Si NC and Er^{3+} ions is a complex, multichannel process. [9, 10] Using a series of time-resolved PL experiments, PL excitation spectroscopy and PL quantum yield determination, it has been shown that the non-resonant Er excitation processes proceed by two different energy transfer mechanisms. A "slow" one, involves the afore-mentioned non-radiative recombination of an e-h pair

in a Si NC accompanied by energy transfer to a nearby Er^{3+} ion, and is relatively well understood. A second, "fast" mechanism takes place within $1\,\mu s$ after a pulsed excitation and has been related either to an intraband relaxation of a hot carrier in a Si NC, analogous to impact excitation by hot carriers in bulk semiconductors, [110, 116, 117] or energy transfer via luminescence centers [118]. While the luminescence center mediated transfer can always occur, the impact ionization path requires enough excess energy of the generated e-h pairs. Since the efficiency of the "fast" process can potentially be much higher than that of the "slow" one, it has an interesting application potential.

Here, we examined the dynamics of Er emission sensitized by Si NCs under different excitation conditions. Two excitation photon energies were used, one below the threshold $E_{\rm th}$, defined by the sum of the Si NC bandgap energy and that of the first excited state of Er^{3+}, and a second one larger than $E_{\rm th}$. For both excitation photon energies a wide range of pump fluences was employed. For the lowest pump fluence the average number of photons absorbed per NC during a pulse was much smaller than 1, to ensure there are no multiple photon absorption events in a single NC during a pulse. [119]

5.2 Experimental details

5.2.1 Sample fabrication

The samples used in this work feature thin-films of Er-doped SiO_2 with Si-NCs prepared by sputter deposition. A sub-stoichiometric film of SiO_2 (with a 17 ± 4 vol% excess Si) was deposited by magnetron RF co-sputtering system, using high purity Si (99.99%) and SiO_2 (99.99%) targets. Moreover, Er is also doped in; for this we place pellets of Er_2O_3 on the sputter targets, and adjust the stoichiometric ratio of Si to SiO_2 according to the added oxygen content due to the Er_2O_3 pellets. After deposition of a $2\,\mu m$ thick SiO_2 layer enriched with Si and Er on a quartz substrate, the layer was annealed at $1200\,^\circ C$ in N_2 atmosphere for 30 minutes to form Si NCs. The Er concentration is $\approx 2.7\ 10^{19} cm^{-3}$. The concentration of Si NCs was determined to be $2.1\ 10^{18} cm^{-3}$ with an average diameter of $3\,nm$. More details on the fabrication process and material characterization can be found in Ref. [107].

5.2.2 Optical characterization

For the time resolved PL excitation experiment, we use the $410 - 710\,nm$ signal of a SOLAR LP603-I Optical Parametric Oscillator (OPO), pumped by the third harmonic of a Nd:YAG LQ629-10 $1064\,nm$ laser, with $100\,Hz$ repetition rate and $\approx 12\,ns$ pulse duration. The excitation flux was adjusted by use of double Glan-Thompson polarizers. The photoluminescence was collected by an optical fiber and directed

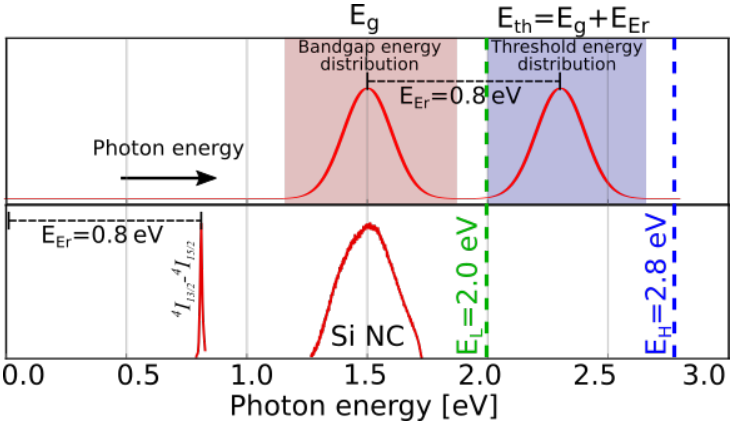

Figure 5.1: Visualization of excitation threshold energy. **Top** An approximate bandgap energy, E_g, and threshold energy, E_{th}, distributions, are shown with the chosen excitation energies, E_L (Dashed green line) and E_H (Dashed blue line). **Bottom** The top energy distribution is shown in relation to the observed photoluminescence spectrum.

through an optical filter in order to select the Er^{3+} emission, and eventually towards a NIR photomultiplier tube (PMT, Hamamatsu R5509-73), ultimately the PMT signal is read out in multichannel scaler mode by a data-acquisition card (Fast Comtec P7887). The photoluminescence spectra of both the Si NCs as well as the Er^{3+} were measured by Horiba Fluorolog-3 spectrometer, with a Xenon lamp as an excitation source, and both a Si CCD and an InGaAs detectors.

5.2.3 Threshold energy, E_{th}

The excitation photon energies below and above the threshold were chosen carefully based on the specific sample studied. Following is the analysis of the choice. We consider the case of a Si NC with bandgap energy, E_g, facilitating excitation of an Er^{3+} ion into its 1^{st} excited state, with the energy E_{Er}. As discussed, the excitation of the Er^{3+} ion by the Si NC, can proceed in two ways. [i] A "slow" excitation, coinciding with the band to band non-radiative recombination of an e-h pair, requiring $E_g > E_{\mathrm{Er}}$. [ii] A "fast" excitation, which we argue happens though the transition of a carrier from a highly excited state with energy E_H to a lower energy state E_L still inside the conduction band. In other words [ii] requires $E_H - E_L = E_{\mathrm{Er}}$.

In our material, an ensemble of Si NCs with a size dispersion, condition [i] will always be valid, but condition [ii] depends on excitation details. The size distribution of the crystals, E_g varies from crystal to crystal. Therefore, E_L (Dashed green line in fig 5.1) should be larger than that of the most energetic crystal in the distribution

in its ground state, and at the same time smaller than the sum (E_{th}) of least energetic crystal in the distribution and first excited state of Er^{3+}. The same kind of reasoning applies for E_H (Dashed blue line in fig 5.1), E_{th} follows the same distribution as E_g, only increased by energy E_{Er}. When exciting above E_{th}, it is necessary to excite with E_H sufficient for the most energetic crystal in the ensemble. Ultimately, this has led to the choice of excitation energies $E_L = 2.0\,eV$ and $E_H = 2.8\,eV$.

5.2.4 Temporal decay analysis

In order to observe the PL time dynamics both on the nanosecond, through the microseconds and up until the Er^{3+} has recombined after several milliseconds, it is necessary to measure with high temporal resolution (bin time varying between $2\,ns - 32\,ns$) as well as long enough detection windows ($\approx 10\,ms$). The temporal resolution was chosen to optimize signal-to-noise ratio, total integration time, and the ability to resolve the shortest features we are interested in. The resulting data-sets are therefore unmanageable in size, containing up to $5\ 10^7$ data-points. The ns-to-ms measured data-set has been averaged in such a way to optimize signal-to-noise ratio as much as possible in all time regimes, but mainly to contain less data points, without losing details in all the observed temporal ranges. Therefore an averaging algorithm has been applied, where the time bins are equidistant on the log time-scale instead of the linear time-scale, spanning over increasingly more datapoints as the measurement advances. This in turn increases the signal-to-noise ratio at later times compared to earlier times.

5.3 Results

Fig. 5.2 shows the different time regimes in the decay dynamics of $1.5\,\mu m$ emission sensitized by Si NCs, observed in time resolved PL over 5 orders of magnitude, from ns to ms. In the first region (α) a fast decay can be observed and has a typical time constant of a few tens of ns. It has been suggested to be due to a combination of defect-related emission and a fast direct excitation of Er^{3+} ions competing with efficient non-radiative processes of energy back transfer from Er^{3+} to the NC core. [5, 118, 120] The second region (β) shows a slower rise, indicating the energy transfer from Si NCs to Er by non-radiative recombination of the e-h pair. The time constant of this rise is determined by the combination of the energy transfer time and the relaxation time from the higher excited states to the 1^{st} excited state of Er^{3+}. The most important contribution to the latter process is that of the $^4I_{11/2}$ to $^4I_{13/2}$ excited state transition, with a time constant of $\sim 2.4\,\mu s$ [118]. Using this value and fitting the rise with rate equations describing the transfer, we find a value of $\sim 10\,\mu s$ for the energy transfer time. The last region (γ) depicts the radiative decay of Er^{3+} ions and has a time constant of $\sim 4\,ms$. As there are no energy transfer processes taking place after

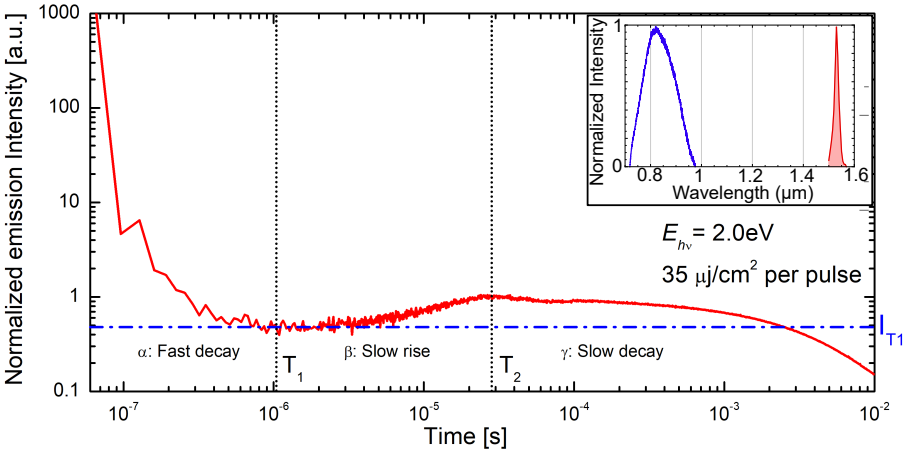

Figure 5.2: Log-log plot of the typical PL dynamics measured at $1535\,\mathrm{nm}$. There are 3 distinct stages: (α) an initial fast decay with a time constant of a few tens of ns. This is followed by (β) a slower rise and finally (γ) a slow decay with a time constant of $4\,\mathrm{ms}$. The emission intensity is normalized at $\mathrm{T_2}$, when the maximum concentration of excited $\mathrm{Er^{3+}}$ ions is observed. The intensity at the minimum, $\mathrm{I_{T1}}$, indicates the excited $\mathrm{Er^{3+}}$ concentration obtained by fast processes which survive the initial fast (nonradiative) decay and contribute to the PL signal, slowly decaying in stage (γ). The inset depicts the normalized emission spectra of the sample with the Si NC emission spectra around $920\,\mathrm{nm}$ (blue) and $\mathrm{Er^{3+}}$ emission around $1535\,\mathrm{nm}$ (red).

all the NCs have transferred their energy, for the remainder of the manuscript we focus on the first $\sim 35\,\mu s$ after the pump pulse. In order to make quantitative comparisons between the different decay kinetics, we set the maximum of the emission intensity around $t = 30\,\mu s$ (I_{T2}) to 1, and determine the value of the lowest part of the emission intensity at $t = 1\,s$ to be I_{T1}, indicative for the Er concentration that is excited by processes faster than that of the "slow" energy transfer, due to the non-radiative recombination of e-h pairs.

We have probed the PL dynamics by two excitation photon energies. The first one being $E_{h\nu} = E_L = 2.0\,eV$, below the threshold value, E_{th}, as discussed in section 5.2.3. The second one above the threshold with a photon energy of $E_{h\nu} = E_H = 2.8\,eV$. In both cases the excitation power was varied to probe the decay kinetics for different excited NCs concentration after the pulse. In Fig. 5.3a the values of I_{T1} are shown as function of average number of absorbed photons per NC, determined following the procedure described in Ref. [5]. We note that I_{T1} is proportional to the population of Er^{3+} ions that are excited via fast processes. We observe that for the case of $E_{h\nu} = 2.8\,eV$, there is no change of I_{T1} for different excitation powers. The contribution of Er^{3+} ions excited by the fast process is about 70% of the total population of excited Er^{3+} ions, over the whole range, from very low excitation flux up to very high. In contrast, for the photon energy of $E_{h\nu} = 2.0\,eV$, the contribution of the "fast" excitation process to the total population of excited Er^{3+} ions goes down for small fluxes, and even completely disappears for the smallest excitation density. We note that the decay kinetics still show a fast ns component, but this does not give rise to any excited Er^{3+} ions which could be observed for longer times, and thus can be completely designated as originating from "defect-related" emission. At larger values of the pump fluence at $E_{h\nu} = 2.0\,eV$, the value of I_{T1} stabilizes at approximately 45% of the total excited Er^{3+} population.

From the results obtained with time resolved PL we can draw the following conclusions: For a low photon fluence at $E_{h\nu} = 2.0\,eV$ there is only one excitation mechanism taking place, which is the "slow" non-radiative recombination of excitons in Si NCs exciting Er^{3+} ions into a higher state, which is then followed by subsequent relaxation to the first excited state. This is distinctively different for the cases where either a high fluence, or a larger photon energy $E_{h\nu} = 2.8\,eV$ are applied. Under both of these pumping conditions, the Er-related PL dynamics are similar, and considerably different to that recorded while pumping at $E_{h\nu} = 2.0\,eV$ at low flux. In the case of the large photon energy there is, next to the "slow" excitation pathway, also the additionally active, "fast" excitation mechanism. This takes place on a short timescale, and its observation in the PL dynamics is obscured by the convolution of Er^{3+} emission with a fast defect-related band at the same detection wavelength. The population of Er^{3+} ions excited by the "fast" process can be distinguished by I_{T1}, as the defect related emission does not contribute to the total PL signal after $1\,\mu s$, and the

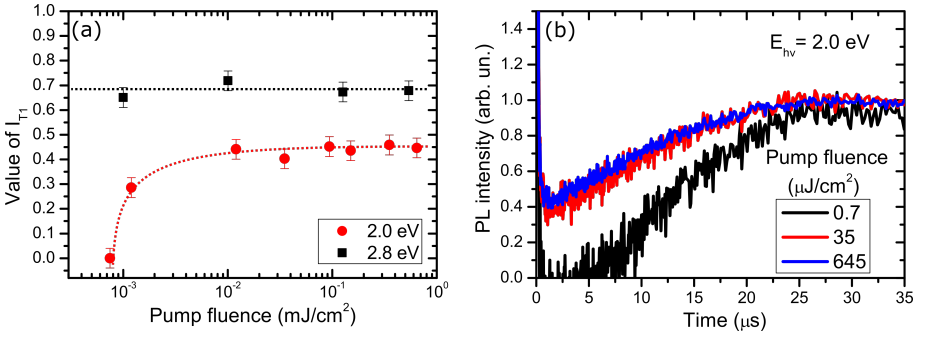

Figure 5.3: (a) Values of I_{T1} as a function of pump fluence for the two excitation photon energies used in this study. The dashed lines serve as guide to the eye. (b) Time-resolved PL intensity for 3 different values of the pump fluence for the first 35 μs for an excitation photon energy of 2.0 eV.

excited Er^{3+} ions have not decayed yet. For a larger pump fluence at $E_{h\nu} = 2.0\,\text{eV}$, a different process can occur giving rise to a similar behavior. This is likely a result of multiple photon absorption in a single NC, followed by an Auger process, in which one e-h pair recombines and transfers its energy to one of the other carriers, effectively creating a "hot" carrier with excess energy, similar as obtained by large energy photon absorption. A schematic of the different excitation conditions and energy transfer processes is depicted in Fig. 5.4.

When we compare our results with that of Refs. [118] and [120], we can see that for the conditions illustrated in Figs 5.4b and 5.4c, we can draw similar conclusions about the relative contribution of the fast and slow process to the excitation of Er^{3+}. However, while in those cases the fast excitation was determined to be mediated by defects / luminescence centers, we explicitly show that this process does not occur in high temperature annealed samples. In this case it is the excess carrier energy, either created by large energy of the absorbed photon, or large number of photons absorbed in the same NC, followed by an Auger process, that is the physical mechanism behind the fast excitation process. We believe that the high temperature annealing creates high quality Si nanocrystals, and removes the defects which can provide an alternative fast excitation channel for Er^{3+} ions in matrices of lesser crystalline quality. Also, because of the longer carrier lifetimes which accompany the good crystallinity, the Auger process becomes possible and gives rise to the hot carrier mediated Er^{3+} excitation process. Although it is difficult to pinpoint the exact reason of the difference in the value of I_{T1} for both photon energies at high flux, there are some comments we can make with might be related to this. Firstly, there might be a difference in the subset of excited NCs due to difference in absorption cross-section at the two photon energies.

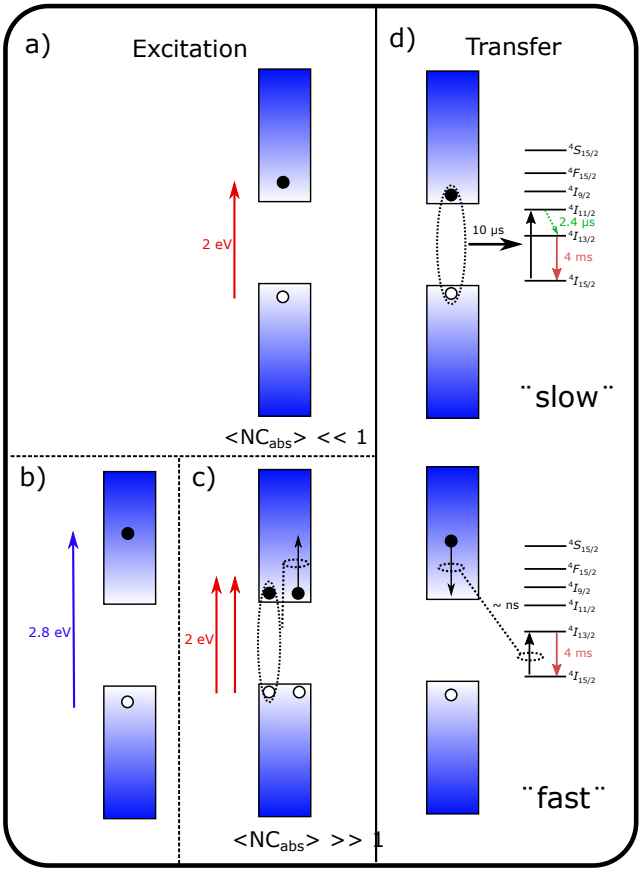

Figure 5.4: Schematics of the different excitation conditions and energy transfer processes from Si NCs to Er^{3+} ions. **(a)** At low pump fluence and small-energy, a single low-energy e-h pair is created in a Si NC. **(b)** Absorption of a high-energy photon leads to generation of high-energy e-h pair. **(c)** Absorption of multiple small-energy photons, at large pump flux, leads to generation of multiple e-h pairs in a single NC. Subsequent recombination of one e-h pair transfers its energy in an Auger process (indicated by the dotted lines), leaving behind a single high-energy e-h pair. **(d)** Energy transfer to Si NCs to Er ions. The slow process takes place upon recombination of a low-energy e-h pair, with a transfer time of $10\,\mu s$, exciting Er^{3+} ions to a higher excited state. A second "fast" process can only occur for the conditions indicated in (b) and (c). Excess energy of a "hot" carrier is transferred by means of impact ionization, exciting Er^{3+} ions directly into the $^4I_{13/2}$ state.

Secondly, in case of $2.0\,\mathrm{eV}$ excitation, we might not have reached the saturation yet, so a subset of Si NCs is still only singly excited and not contributing to I_{T1}, leading to its smaller value. This effect will be additionally enhanced by the inhomogeneity of the laser excitation spot.

5.4 Conclusion

We have used time-resolved PL to probe the energy transfer dynamics of Si NCs to Er^{3+} ions in Er-doped Si rich SiO_2 films. By using two excitation energies, one below the threshold value determined by the sum of the Si NC bandgap and 1^{st} excited state of Er^{3+}, and the other one above, we demonstrated that at low pump fluence the fast (sub µs) excitation process does not take place below the threshold pump photon energy. This explicitly demonstrates that there is no "defect" mediated direct excitation process active in our materials. Furthermore, we demonstrate that an additional excitation pathway by hot-carrier-mediated impact becomes activated as soon as there are carriers available with sufficiently large excess energy. These can be created by absorption of above energy threshold photons, or by the absorption of multiple sub-threshold photons in a single NC followed by an Auger process. In both cases the kinetics are nearly identical and the contribution to the total excited Er^{3+} population is for the largest part a result of the hot carrier mediated pathway, which is responsible for $45 \sim 70\%$ of the total population of excited Er^{3+} ions. These results show the importance of choosing the right excitation conditions for this system, and offer a viable pathway for reaching population inversion, and possibly lasing, in SiO_2:Er sensitized with Si-NCs.